Measurement of Lateral Resolution in Confocal Raman Spectroscopy Using Indium Arsenide Nanowires

Journal of Raman Spectroscopy

WILEY

Journal of RAMAN SPECTROSCOPY

RESEARCH ARTICLE OPEN ACCESS

Measurement of Lateral Resolution in Confocal Raman Spectroscopy Using Indium Arsenide Nanowires

Sebastian Wood[1] | Keith R. Paton[1] | Ruth Rawcliffe[2] | Tomas Peach[2,3] | Tehseen Adel[4] | Alessio Sacco[5] | Hugo Kerdoncuff[6,7] | Matthieu Paillet[8] | Ahmed-Azmi Zahab[8] | Paul Finnie[9] | Li-Lin Tay[10] | Jeongyong Kim[11] | Hyuksang Kwon[12] | Nobuyasu Itoh[13] | Shinsuke Kashiwagi[14] | Andrea Mario Rossi[5] | Yaxuan Yao[15] | Lingling Ren[15] | Elif Ozçeri[16] | Gemma Rius[16] | David Steinmetz[17,18] | Andrea Richter[17] | Thomas Dieing[17] | Agnès Tempez[19] | Ophelie Lancry[19] | Marc Chaigneau[19] | Angela R. Hight Walker[4] | Erlon H. M. Ferreira[20] | Maxim Shkunov[2] | Fernando A. Castro[1,2]

[1]National Physical Laboratory (NPL), Teddington, Middlesex, UK | [2]Advanced Technology Institute, Faculty of Engineering & Physical Sciences, University of Surrey, Guildford, UK | [3]Institute for Compound Semiconductors, Cardiff University, Translational Research Hub, Cardiff, UK | [4]Physical Measurement Laboratory, National Institute of Standards and Technology (NIST), Gaithersburg, USA | [5]Quantum Metrology and Nanotechnology Department, Istituto Nazionale di Ricerca Metrologica (INRiM), Torino, Italy | [6]DFM Danish National Metrology Institute, Hørsholm, Denmark | [7]NKT Photonics, Birkerød, Denmark | [8]Laboratoire Charles Coulomb, Université de Montpellier, CNRS, Montpellier, France | [9]Quantum and Nanotechnologies Research Centre, National Research Council Canada, Ottawa, Ontario, Canada | [10]Metrology Research Centre, National Research Council Canada, Ottawa, Ontario, Canada | [11]Department of Energy Science, Sungkyunkwan University, Suwon, Republic of Korea | [12]Korea Research Institute of Standards and Science (KRISS), Daejeon, Republic of Korea | [13]National Metrology Institute of Japan (NMIJ), National Institute of Advanced Industrial Science and Technology (AIST), Tsukuba, Japan | [14]HORIBA Japan, Kyoto, Japan | [15]Technology Innovation Center of Graphene Metrology and Standardization, State Administration for Market Regulation, National Institute of Metrology (NIM), Beijing, People's Republic of China | [16]Institute of Microelectronics of Barcelona, IMB-CNM (CSIC), Barcelona, Spain | [17]Oxford Instruments, WITec, Ulm, Germany | [18]Bruker Optics GmbH & Co. KG, Ettlingen, Germany | [19]HORIBA France, Palaiseau, France | [20]INMETRO National Institute of Metrology, Quality and Technology (Inmetro), Rio de Janeiro, Brazil

Correspondence: Sebastian Wood (sebastian.wood@npl.co.uk)

Received: 8 May 2025 | **Revised:** 2 September 2025 | **Accepted:** 17 September 2025

Funding: This work by NPL received funding from the UK Department for Science, Innovation and Technology (DSIT) through the National Measurement System. The work undertaken by NIM was supported by the National Key R&D Program of China (Nos. 2022YFF0608600 and 2016YFF2024300). Work undertaken at DFM was funded by the Danish Agency for Institutions and Educational Grants. NIST work was funded solely by the United States Government. The authors acknowledge technical advice on the protocol development from Andrew Pollard, Caitlin Thomson, Filipe Richheimer and Alexander G. Shard (NPL).

ABSTRACT

Lateral resolution is a key figure of merit for spectroscopy across all applications. Confocal Raman spectroscopy is able to provide chemical and structural information with submicrometre resolution, resulting in widespread use across multiple disciplines of science and technology. However, the lack of agreed-upon measurement standards and appropriate reference samples has hindered uptake. Here, we report the development and demonstration of a reference sample based on indium arsenide (InAs) semiconducting nanowires for measuring the lateral resolution of confocal Raman spectroscopy with a pathway for traceability to the International System of Units (SI). An interlaboratory comparison involving 15 participants from 11 countries has been conducted to rigorously test and demonstrate the suitability of the sample and the method. The study identified required revisions to the measurement protocol to improve the consistency of data analysis and that the long-term operational stability of the reference sample requires further improvement. Based on a revised data analysis protocol, the method delivered consistent results at the 95% confidence level for eight of the nine participants who returned full datasets. Outcomes from this study have contributed to the publication of a new international standard (ISO 23124:2024).

1 | Introduction

Raman spectroscopy is a widely used technique for the characterisation of materials and samples across a broad range of disciplines for research, industry and clinical applications [1–4]. However, results obtained in different laboratories cannot be consistently compared due to the lack of appropriate measurement standards and calibration methods. Growing demand for interoperable systems, reference spectra databases and quantitative analysis requires the development of methods for reliably calibrating measurements [5–9]. A recent review of existing standards for Raman spectroscopy has highlighted multiple areas of need within the field and identifies spatial resolution and laser spot profiling as areas for development [10].

Confocal Raman spectroscopy offers chemical and structural sensitivity with submicrometre spatial resolution and is widely used for the analysis of microstructured materials in fields such as life sciences, materials science, condensed matter physics, analytical chemistry and microelectronics. Lateral resolution is a key figure of merit for comparing the performance of instruments and measurement parameters. In principle, the spatial resolution achieved is diffraction-limited so it allows lateral resolution of less than 1 μm for visible light. Whilst this value is often quoted, such claims are rarely substantiated due to the lack of suitable agreed-upon measurement methods. Lateral resolution in this manuscript refers to the minimum separation of spatial features such that they can be distinguished. The Rayleigh criterion is the most common approach to determining this resolution (though other criteria may be applied) [11]. Irrespective of the criterion for distinguishing features, these methods all relate to the spatial point-spread function (PSF) of the measurement. For confocal spectroscopy, it is important to remember that the PSF of the measurement is not the same as the laser spot size since the confocal light collection also contributes to the spatial resolution [12].

There are several approaches for measuring the lateral spatial resolution of a 'beam-based' method like confocal spectroscopy, and these are comprehensively described in the ISO 18516:2019 standard [11, 13, 14]. The typical approach is to measure the spatial profile of the signal from a feature much smaller than the beam diameter. The measurement of a point-like feature results in an approximation of the PSF, or alternatively, a sharp linear feature gives an approximation of the line-spread function or edge-spread function [15]. Each of these can be used to estimate the spatial resolution of a measurement. However, a challenge in applying these methods to Raman spectroscopy is the lack of suitable measurement artefacts, which would require the following characteristics:

- Clearly defined features with structures much smaller than the expected lateral resolution (i.e., significantly smaller than 1 μm);
- Strong Raman scattering signal providing clear contrast with the background;
- Robust sample able to withstand prolonged and repeated laser exposure; and
- Features that can be easily located and whose spatial dimensions can be traceably measured.

In this study, a candidate sample is considered comprising indium arsenide (InAs) nanowires aligned between metal pads, which can be used for a line-spread function measurement of spatial resolution. InAs nanowires were chosen on the basis of a strong Raman scattering signal and the availability of a batch of nanowires with an appropriate average diameter. We consider the use of a green (532-nm wavelength) excitation laser, which is commonly used. In principle, the method equally applies to other excitation lasers; however, shorter wavelengths would be subject to greater uncertainties arising from the finite dimensions of the reference sample.

A measurement protocol has been developed and tested through an interlaboratory comparison with 15 institutions. The results demonstrate the general suitability of this method for measuring lateral resolution but reveal specific challenges related to the consistency of data analysis and handling of background signal. This was addressed by updating the protocol and re-analysing raw data from participants to demonstrate improved reliability of the revised protocol. The study also identified a limitation arising from polarisation-dependent laser-induced degradation of the InAs nanowires used in this study, which restricts the range of applications and suggests the need to adopt an alternative nanowire material.

2 | Experimental Methods

2.1 | Sample

The sample design, represented in Figure 1a, offers the unique identification of individual nanowire features to enable metrological traceability by defining pairs of tapered macroscopic gold electrodes deposited on an array of aligned nanowires such that the nanowires span the gap between the closely spaced narrow ends. The overall substrates are roughly 25-mm squares with 40 electrode pairs each. A photograph of a sample is provided in Supporting Information (Appendix B). Preparation of these samples was achieved using the dielectrophoresis method for aligning semiconducting nanowires from suspension onto electrode gaps that have been previously reported [16, 17]. Scanning electron microscopy (SEM) was used to examine the sample, and Figure 1b presents an example where a single nanowire is clearly resolved between a pair of metal pads. Atomic force microscopy (AFM) was also used for a quantitative measurement of the nanowire dimension, and an example of a topography profile is given in Figure 1c. Since nanowires may have nonuniform diameters, five topography profiles were taken to give an average; in this case, the measured diameter is 72 ± 7 nm, which is consistent with the nominal batch diameter of 100 nm (see Table 1).

Five samples were prepared and screened using optical microscopy (Figure 1d presents an example micrograph) to identify electrode gaps containing straight nanowires that bridge the whole gap. Two features (referred to as A and B) on each sample were selected and examined in detail using AFM to measure the dimensions of the individual nanowires. In this case, a research instrument was used, relying on a reference artefact for dimensional calibration, but a metrological AFM could be used to establish traceability to the SI metre [18]. The dimensions

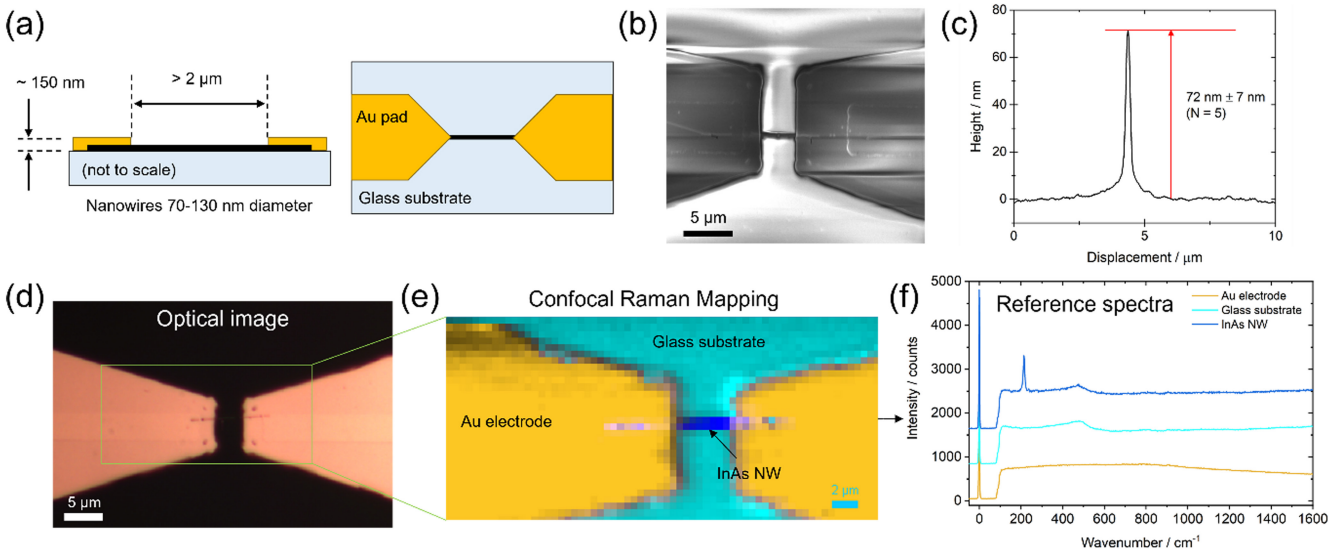

FIGURE 1 | (a) Schematic illustration of the inorganic nanowire features used for the lateral resolution measurement. (b) SEM image, (c) AFM topography profile and (d) optical microscope image showing examples of the nanowire features. (e) Confocal Raman mapping of the feature shown in (d) using classical least squares model to represent different materials with the reference spectra shown in (f), note the strong photoluminescence background and edge filter cut-off at around 100 cm^{-1}.

TABLE 1 | Nanowire diameter measurements using AFM for Feature A and Feature B on each of the five samples. Sample 2 had only one useable feature, so it was only used for protocol development. Uncertainty reported at 68% confidence ($k = 1$).

	Feature A diameter [nm]	Feature B diameter [nm]
Sample 1	101 ± 33	125 ± 6
Sample 2	72 ± 7	N/A
Sample 3	106 ± 2	167 ± 23
Sample 4	126 ± 3	303 ± 33
Sample 5	117 ± 5	153 ± 7

of these nanowires are provided in Table 1, taken from AFM measurements provided in Supporting Information (Appendix A). The nanowire diameter measurement and uncertainty were evaluated by taking the mean and standard deviation of values extracted from five AFM line profiles across the nanowire at different positions. For each sample, a narrow nanowire was designated Feature A for use as a resolution measurement artefact, and a thicker nanowire (or clustered pair) was designated Feature B for use as a test artefact.

Further demonstration of the sample suitability is provided using confocal Raman spectroscopy for the region of interest shown in Figure 1d. Figure 1e shows a false colour mapping of Raman signatures based on a classical least squares (CLS) model with three reference spectra presented in Figure 1f. The gold electrode shows a flat spectrum on a sizeable background with no Raman peaks; the glass substrate has a weak Raman peak at around 470 cm^{-1} from the silica, whereas the InAs nanowire exhibits a characteristic transverse optical mode peak at around 212 cm^{-1} [19, 20].

2.2 | Interlaboratory Comparison Protocol

Interlaboratory comparisons are recognised as an important step towards the creation and international acceptance of new documentary standards. In this case, the intercomparison was supported by the VAMAS (Versailles Project on Advanced Materials and Standards) organisation, which is a global initiative supporting prestandards research for advanced materials [21]. The interlaboratory comparison was designed to test the suitability of the proposed measurement protocol and samples provided. Since each laboratory used its own instrument and personnel, it was necessary that all participants followed the same measurement protocol and that all the measurements used the same set of samples, which were circulated between participants. Four samples were circulated by the lead participant, starting in different global regions with the intention that each would be passed to a new participant with up to 3 months to perform measurements and then pass the sample on. The samples were distributed in January 2020, shortly before the COVID-19 pandemic, which resulted in major delays to the project and loss of samples. To compensate for those losses, the remaining samples were circulated to additional participants, and the final datasets and samples were returned in November 2023.

The full measurement protocol for the interlaboratory comparison is provided in Supporting Information (Appendix B). To summarise, the protocol describes the measurement of the Raman spectrum as a linear profile perpendicularly across the nanowire feature. At each spatial position, a Raman spectrum is acquired (such as that in Figure 2a), and the signal is integrated across the spectral range of interest (in this case, 150 to 310 cm^{-1}). The resulting intensity profile then has a peak whose width is representative of the measurement lateral resolution (as exemplified by Figure 2b). The profile is then fitted with a Gaussian peak whose Full Width Half Maximum (FWHM) is taken as the

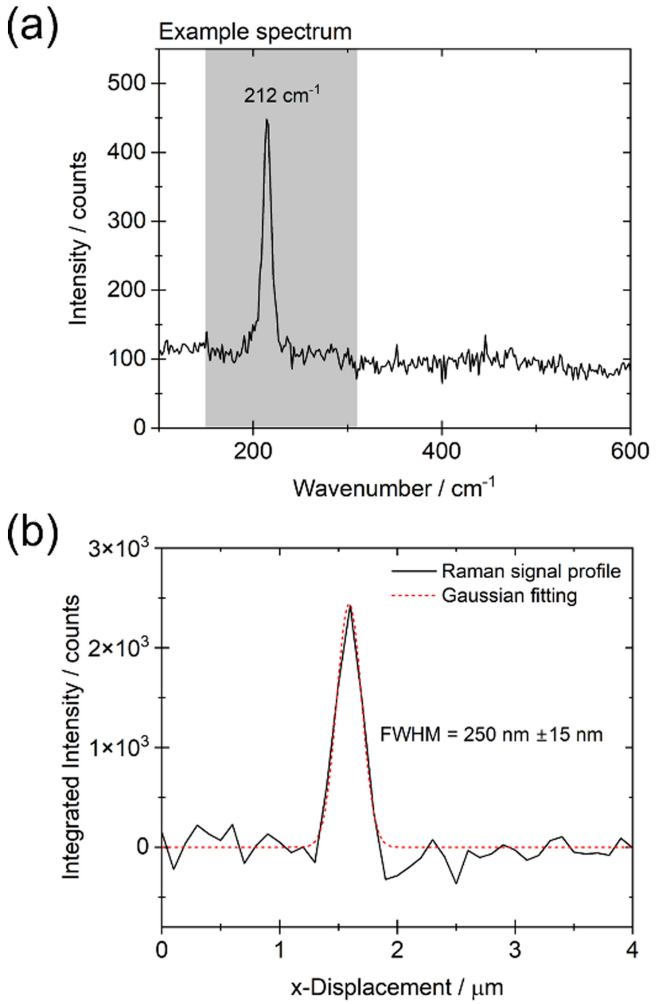

FIGURE 2 | (a) Example Raman spectrum from an InAs nanowire with a characteristic Raman peak at 212 cm^{-1}. (b) Intensity of the integrated signal over the spectral range of 150–310 cm^{-1} (shaded in b) plotted as a displacement profile perpendicular to the nanowire. Red trace shows fitting of a Gaussian profile with FWHM of 250 nm.

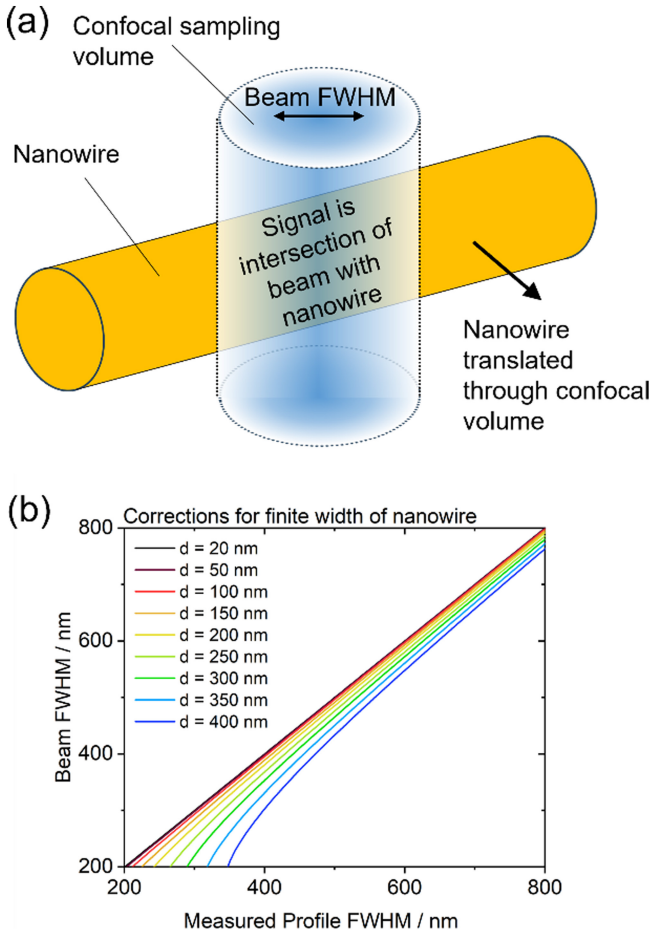

FIGURE 3 | (a) Schematic illustrating the numerical model used to simulate the effect of nanowire diameter on the width of the spectroscopic mapping profile. (b) Plot of simulated results showing relationship between the apparent 'Measured profile FWHM', and the actual 'Beam FWHM' for a range of nanowire diameters from 20 to 400 nm.

measure of spatial resolution (in this case, 250 ± 15 nm) with the standard uncertainty arising from the fitting.

The protocol required each participant to measure five profiles across each nanowire feature to take an average and also included measurements with the nanowire oriented in two perpendicular directions (x and y) to give separate measurements of the lateral resolution in each axis. Furthermore, the protocol included measurements using different positions on the sample mapping stage to check for nonlinearities in the travel, but the results did not clearly indicate any such problems, and the simple average over all the measurements has been used throughout this report.

An important aspect of the experimental design was the aim to test the suitability of the measurement protocol rather than to compare the lateral resolutions achieved by each participant. This was achieved by using Feature A and Feature B as measurement and test artefacts, respectively. For this reason, the dimensions of Feature B were withheld from the participants for the duration of the study. The evaluation criterion was therefore the consistency of the lateral resolution measurements between Feature A and Feature B as reported by each participant. Since the Feature B nanowires were thicker, a correction was required to compensate for the thickness variations and make a meaningful comparison.

The nanowire thickness correction was evaluated using a numerical simulation in MATLAB [22]. The confocal volume sampled by the measurement was considered as a cylinder with a Gaussian cross-section (on the basis that the axial resolution of the confocal PSF is much greater than the nanowire diameter). Note that this correction relates only to the finite size of the nanowire and not the effect of defocussing. The nanowire was modelled as a homogeneous cylinder, and the total signal from a measurement was taken as the integral of the confocal volume for all points intersected by the nanowire on a 1-nm pitched 3D Cartesian grid. The model is illustrated schematically in Figure 3a. The signal was calculated for a series of lateral displacements of the nanowire to simulate the intensity profile of the experimental measurement, and the resulting profile was fitted with a Gaussian to extract the FWHM. In this way, the FWHM of the profile in

the simulated measurement was evaluated as a function of the width of the confocal measurement volume (taken as the Gaussian FWHM) for a range of nanowire diameters from 20 to 400 nm. These results are presented in Figure 3b. As expected, for a thin nanowire (20-nm diameter), the width of the measured spectroscopic intensity profile is a good measure of the sampling beam profile (and hence lateral resolution), as shown by a linear trend with unity slope. However, as the nanowire diameter increases, the measured profile becomes an overestimate of the measurement resolution, with the greatest impact for smaller beam profiles (in this case, the nonlinearity is most obvious for measured FWHM < 400 nm). The Feature A nanowires used in this study (see Table 1) all have diameters less than 150 nm, and the modelling results show that this therefore contributes less than 10% uncertainty to the measured lateral resolution for the whole diffraction-limited regime. For the thicker Feature B nanowires, this model is used to apply the correction for the nanowire diameter in evaluating the protocol.

2.3 | Instrument Details

AFM was performed using an AIST Combiscope 1000 in non-contact mode with OPUS 240AC-NN probes, and calibration was achieved using a MikroMasch TGXYZ01 grating. Raman spectroscopy for protocol development and detailed analysis of the samples, as well as optical imaging, was performed using a HORIBA LabRAM HR-800 microspectrometer with a ×100, N.A. = 0.9 objective. The laser excitation wavelength was 532 nm with a laser power ranging from 33 to 3.3 mW measured at the sample plane; the instrument was used without a half-wave plate or analyser for polarisation control. For the polarisation-dependent laser damage threshold measurements, the same instrument configuration was used and the polarisation controlled simply by rotating the sample with respect to the linearly polarised laser excitation. This method mirrors the relevant measurement conditions and also maintains the polarisation state of the excitation laser to enable direct comparison between degradation conditions. However, we note that rotating the sample

TABLE 2 | Instrument details for participants.

Participant	Instrument	Laser wavelength (nm)	Objective	Grating (mm^{-1})	Spectrometer length (mm)	Polariser/ analyser
1	HORIBA LabRAM HR-800	532	100×, 0.9 NA	600	800	None
2	Witec Alpha 300	532	100×, 0.9 NA	1800	300	None
3	Witec Alpha 300	532	100×, 0.9 NA	1800	300	None
4	Home-built with Princeton Instruments Acton SP2500	532	100×, 0.9 NA	1800	500	Analyser
5	Thermo Scientific DXRxi	532	100×, 0.9 NA	1200	225	None
6	HORIBA LabRAM Soleil	532	100×, 0.9 NA	600	320	None
7	Renishaw inVia	514.5	50×, 0.75 NA	2400	250	None
8	HORIBA LabRAM HR-Evolution	532	100×, 0.9 NA	300	800	None
9	HORIBA LabRAM HR-Evolution	532	100×, 0.9 NA	300	800	None
10	HORIBA LabRAM HR-800	532	100×, 0.9 NA	600	800	None
11	HORIBA XploRA Plus	532	100×, 0.9 NA	2400	200	None
12	HORIBA LabRAM HR-800	457	100×, 0.9 NA	600	800	None
13	Home-built with Andor Kymera 328i spectrometer	532	50×, 0.65 NA	600	330	None
14	Witec Alpha 300 A/R	532	100×, 0.95 NA	600	300	None
15	HORIBA LabRAM HR-Evolution	532	100×, 0.9 NA	600	800	None

complicates the comparison of the scattered signal intensities due to the polarisation sensitivity of the spectrometer.

SEM was performed with a TESCAN MIRA system at 5 kV using the In-Beam secondary electron detector with a 9-mm working distance.

For the lateral resolution measurements, each participant used their own instrumentation as indicated in Table 2.

3 | Results and Discussion

The measurement results returned by all the participants are presented in Figure 4a, including the correction applied for the widths of the nanowires (based on the modelled results presented in Figure 3). Results are presented for 15 participants, where Participant 1 is the lead partner (NPL) who only measured Feature A. Participants 2, 3 and 6 also did not return complete datasets. In general, the lateral resolution of confocal

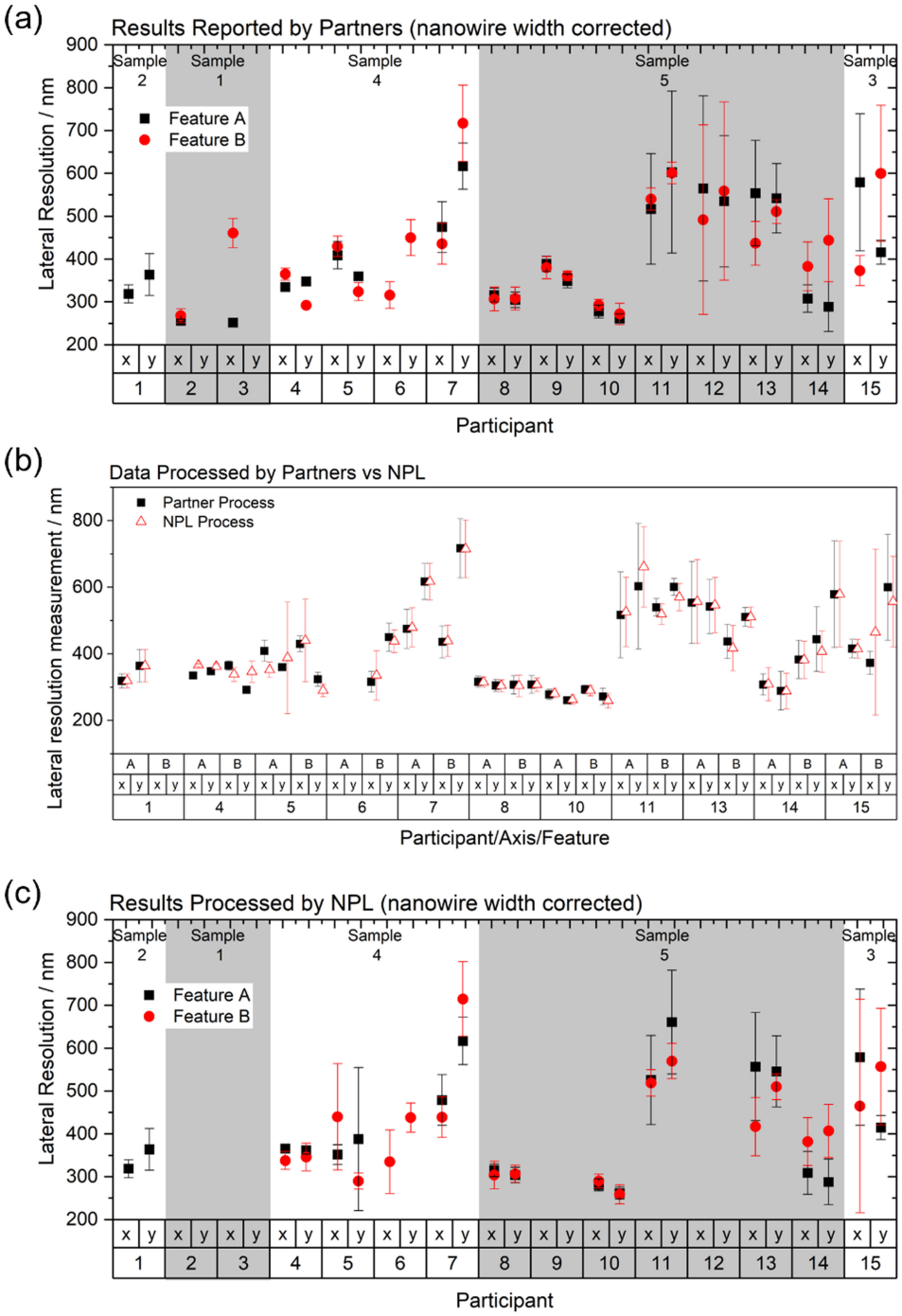

FIGURE 4 | (a) Lateral resolution results as reported by the participants, including the correction for finite nanowire width comparing values for Feature A and Feature B in each case. (b) Comparison of lateral resolution values obtained by participants and values obtained by the project lead reprocessing the raw data. (c) Lateral resolution results following reprocessing of raw data by project lead comparing values for Feature A and Feature B in each case. Note that not all participants provided raw data.

microscopy is quoted as $< 1\,\mu m$, and the theoretical minimum lateral resolution for a confocal spectrometer is estimated by $0.4\lambda / NA$, giving a value of ~236 nm for a wavelength (λ) of 532 nm and a numerical aperture (NA) of 0.9. All of the results returned lie within this range. In some cases, the resolution values measured in the x and y directions are distinctly different, e.g., Participants 6 and 7, indicating that the PSF of the measurement is asymmetric and hence revealing a misalignment of the optical path or that the laser beam profile is not Gaussian.

In principle, the lateral resolution measurements for Feature A and Feature B should agree, and in most cases, they do based on the standard uncertainty (evaluated as the standard deviation with coverage factor, $k = 1$) range indicated on the plot. However, Participants 3, 4 and 15 do not achieve this. In some cases, the uncertainty is large (Participants 11, 12, 13 and 15), also indicating a problem with the protocol. Inconsistencies in the results can arise either from the measurement itself or from the data analysis. To test this, the raw data was reprocessed by the lead participant using the same script for all the data. Most participants had provided full or partial sets of raw data in a usable form, and the results of this reprocessing are presented in Figure 4b. In most cases, the difference is minimal, but for Participants 4, 5 and 15, the mean value moves outside the original uncertainty range. After this reprocessing, the level of agreement is improved, as shown in Figure 4c, noticing in particular that Participants 4 and 15 now exhibit greater consistency between the Feature A and Feature B measurements. However, the difference between results from data analysis by the individual participants and the lead participant with the same dataset indicates an inadequacy of the protocol.

As part of the interlaboratory comparison, participants were invited to comment on any problems with the implementation of the protocol and to suggest improvements. The original protocol assumed that there was no variation in background signal and did not implement a baseline subtraction on the Raman spectrum. However, some participants did detect a substantial background photoluminescence signal in some measurements, which was a major cause of inconsistency in the data analysis. The problem is exemplified in Figure 5a, where the black trace shows a signal intensity profile across a nanowire feature that has two prominent peaks. The inset shows a spectrum corresponding to the larger left-hand intensity peak (plotted in green), which shows a broad background signal but no Raman peak, whereas the spectrum from the smaller right-hand intensity peak (plotted in pink) shows the Raman peak with minimal background signal. The resulting Gaussian fit corresponds to the larger background photoluminescence signal rather than the intended Raman signal.

The origin of this photoluminescence signal is presumably organic contamination on the glass surface, which can be minimised through careful handling but can also be mitigated against by implementing a simple background subtraction in the data analysis. To achieve this, a revised protocol was developed applying a background subtraction across the range of interest (150 to 310 cm^{-1}) by taking averages of 25 data points from either end of the range to fit a linear baseline, as shown in Figure 5b. A related comment from participants was that it was difficult to evaluate the signal-to-noise ratio without extensive analysis of the data, so the revised protocol describes an evaluation of the signal-to-noise ratio from the Raman spectrum of the nanowire directly so that it can be tested during the measurements rather than in postprocessing. The revised protocol is provided in full in Supporting Information with the revisions highlighted (Appendix C).

This improved protocol with the background signal correction was applied to the raw datasets provided by participants (10 datasets from participants plus the lead partner), and the impact on the results is shown in Figure 6a. In most cases, the new protocol gives similar results to the original protocol, but for some datasets, there is a substantial difference (e.g., Participants 5, 7, 11 and 15).

Figure 6b compares results for Feature A and Feature B based on the revised protocol. Out of the 11 participants who provided raw data, nine included both features enabling a quantitative

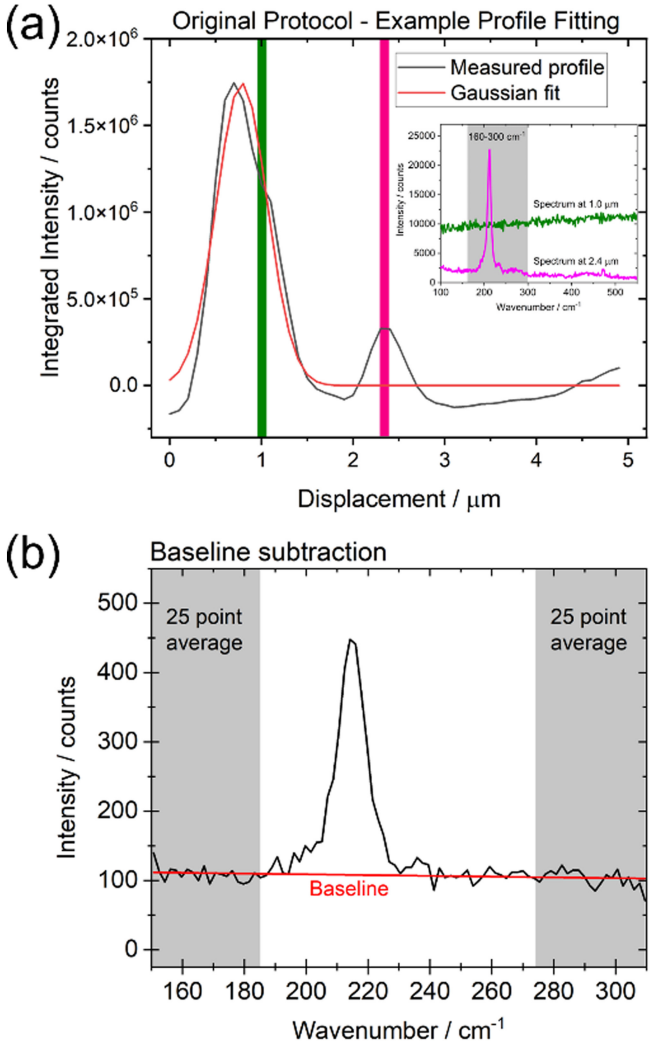

FIGURE 5 | (a) Example Raman intensity profiles based on the original protocol where the Gaussian fitting is dominated by the background signal rather than the Raman signal. Inset shows example spectra, where the green spectrum is dominated by the background signal, and the pink spectrum is dominated by the Raman signal. (b) Example of baseline subtraction for the revised protocol.

comparison. Of these nine, five of them show agreement within the standard uncertainty bars for both *x*- and *y*-resolutions (Participants 4, 5, 8, 10 and 15) whereas four do not (Participants 7, 11, 13 and 14). To aid comparison, the difference in lateral resolution measurements for Feature A and Feature B is plotted in Figure 6c. In this plot, the uncertainty is plotted at both the 68% ($k=1$) and 95% ($k=2$) confidence levels, and a difference value of zero is expected. At the 68% confidence level, results from Participants 7, 13 and 15 fall outside the uncertainty interval: however, at the 95% expanded confidence level, all the results, except for the *x*-axis measurement for Participant 7, are consistent (representing eight out of nine participants who returned full datasets), demonstrating the overall success of this measurement protocol. However, many of the uncertainty ranges are large and hence indicate underlying challenges for this measurement.

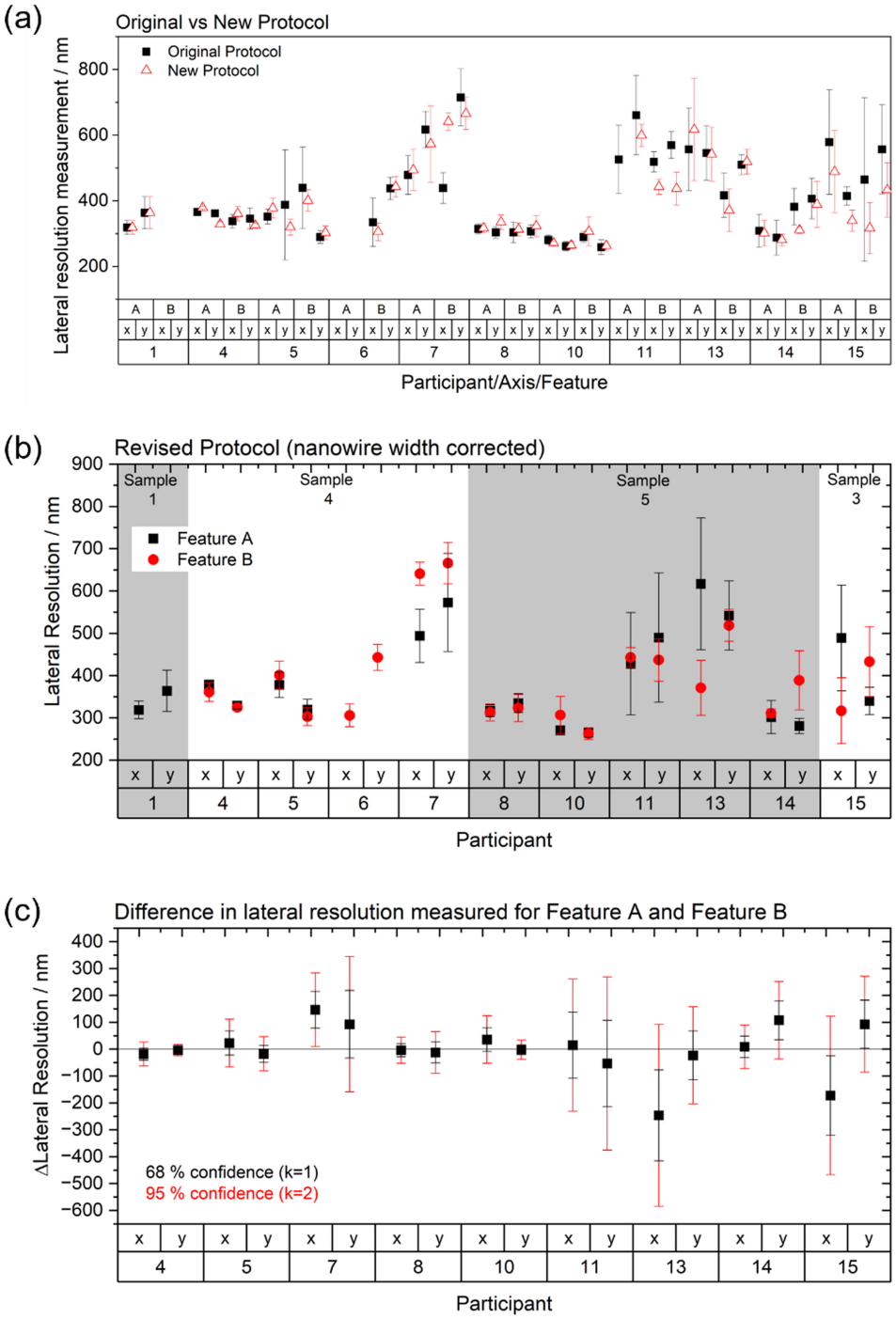

FIGURE 6 | (a) Comparison of lateral resolution values obtained using the original protocol and the revised protocol based on raw data provided by participants. (b) Lateral resolution results based on the revised protocol to suppress background signal comparing values for Feature A and Feature B in each case. (c) Difference values between lateral resolution measurements for Feature A and Feature B for each participant with standard uncertainties indicated at the 68% ($k=1$) and 95% ($k=2$) confidence levels. Note that not all participants provided raw data.

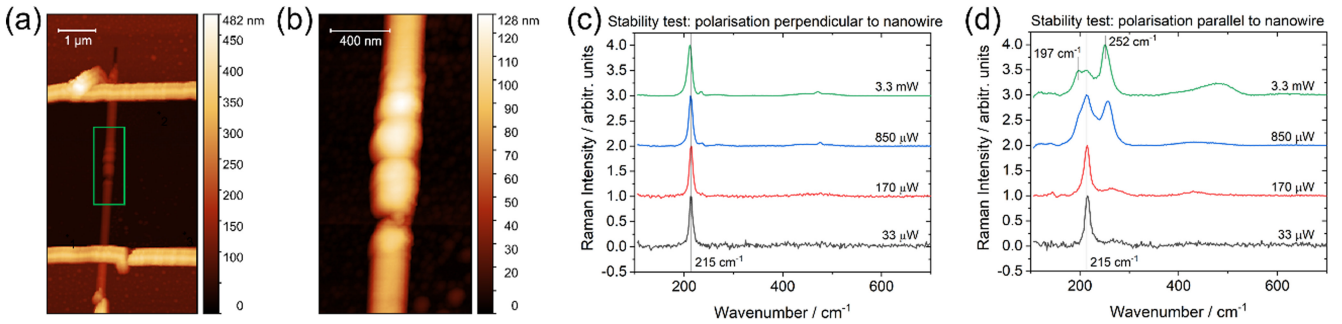

FIGURE 7 | (a) AFM topography image of a damaged nanowire returned to NPL (Sample 5). (b) Detail of the damaged nanowire region corresponding with green box in (a). Normalised Raman spectra measured for an InAs nanowire for different laser powers to test stability with laser polarisation (c) perpendicular and (d) parallel to the nanowire axis.

In general, the participants that achieved the closest agreement between the two sets of measurements are also those that measured the smallest lateral resolutions with narrow uncertainty ranges and comparable values in both *x*- and *y*-resolutions. In contrast, the participants with inconsistent results tend to exhibit larger lateral resolution measurements with broader distributions. This may indicate differences in local practices or instrument capabilities, particularly in achieving an optimised focus on the reference sample. Several participants highlighted the challenge of focusing the instrument accurately on the nanowire, which is consistent with this observation. Another potential limitation is instability in the reference samples themselves. Two of the samples were circulated to multiple participants (Samples 4 and 5), resulting in a large number of measurements being performed in sequence. There is some indication in the results that the initial measurements gave narrower distributions of lateral resolution measurement than the later ones, which may arise from sample degradation. One participant also reported evidence of damage to one of the nanowires, and the sample (Sample 5) was returned to NPL for analysis.

Damage to the nanowire was reviewed using AFM, and the results are presented in Figure 7. The topography map shows a series of breaks in the InAs nanowire accompanied by local increases in the height and width of the nanowire. This is consistent with laser-induced damage arising during a series of line-profile spectral measurements across the nanowire. This indicates that the laser power damage threshold has been systematically exceeded and prompted a closer examination of the stability of the nanowires. Raman spectra were recorded for a nanowire feature at a range of laser powers from 33 to 3.3 mW (each with 1-s exposure and starting with a fresh region of the sample).

The effect of laser polarisation was considered by rotating the sample by 90°, and results are plotted in Figure 7c,d. For the laser polarisation perpendicular to the nanowire axis, all the spectra show the characteristic Raman peak at 215 cm^{-1} with no sign of degradation. However, with the laser polarised parallel to the nanowire axis, the spectra show the appearance of additional Raman peaks at around 197 and 252 cm^{-1}, as well as a broader feature centred around 440 cm^{-1}. These changes in the spectrum appear for laser powers between 170 and 850 µW, demonstrating that the laser damage threshold is much lower for this polarisation of excitation. The new Raman peaks are characteristic of crystalline As and therefore indicate photothermal oxidation of InAs resulting in loss of In from the nanowire crystal, probably as an oxide [19, 20, 23]. It is known that semiconductor nanowires exhibit stronger optical absorption for excitation polarised parallel to the axis, which can explain why the laser-induced damage threshold is lower in this case [23, 24]. Polarisation control in Raman spectroscopy is widely used for nanowire studies but requires a careful approach to accurately evaluate the polarisation state of the optical excitation and collection efficiency of scattered light; however, this is beyond the scope of the present study [10, 25].

Clearly, the instability of the InAs nanowires to laser excitation poses a limitation on their utility as a reference sample, and the polarisation dependence demonstrates that the laser damage threshold is an order of magnitude lower than described in the original measurement protocol. The revised protocol therefore has a reduced maximum laser power, but this is detrimental to the signal-to-noise ratio, resulting in longer measurement acquisition times. An alternative approach would be to replace the InAs nanowires with a more stable material such as silicon.

4 | Conclusions

This interlaboratory comparison project developed and evaluated a protocol for measuring the lateral resolution achieved in confocal Raman microscopy. The method is based on a line-spread measurement using aligned nanowires of InAs that can be individually identified and repeatably measured. In principle, this enables the measurement of lateral resolution to deliver metrological traceability to the SI using a metrological AFM. The method can be used to measure lateral resolution in both *x*- and *y*-axes to evaluate asymmetry in the measurement spot and hence diagnose optical alignment problems. Robust measurements of lateral resolution are important for the quantitative evaluation of dimensional features in samples and also provide a figure of merit for the performance of different measurement systems.

The interlaboratory comparison with 15 participants from 11 countries demonstrated the suitability of the proposed method but highlighted specific problems with the handling of the Raman spectrum baseline and the laser damage threshold. The

protocol has been revised to resolve these issues, which led to improved consistency of results. An outstanding challenge is that the method remains sensitive to the variability in the focusing of the instrument by the local user. As a result, the lateral resolution measurement values are not solely attributed to the instrument itself but also incorporate local procedures and human factors, which indicate a need to develop further detailed guidance for instrument users. Results from this project have been incorporated into a new international standard (ISO 23124:2024) published in 2024 [26].

Author Contributions

S.W. and F.A.C. devised and planned the work. R.R., T.P. and M.S. prepared the samples. S.W., K.R.P., P.F., L.-L.T., A.R.H.W., E.H.M.F. and F.A.C. contributed to the development of the initial protocol. T.A., A.S., H.K., M.P., P.F., L.-L.T., J.K., H.K., N.I., A.M.R., S.K., Y.Y., L.R., A.T., E.O., G.R., D.S., A.T., O.L., M.C., A.R.H.W. and E.H.M.F. performed measurements using the protocol. S.W. coordinated the interlaboratory comparison, analysed the results and prepared the figures. All authors contributed to the technical discussion and preparation of the manuscript.

Acknowledgements

This work by NPL received funding from the UK Department for Science, Innovation and Technology (DSIT) through the National Measurement System. The work undertaken by NIM was supported by the National Key R&D Program of China (No. 2022YFF0608600 and No. 2016YFF2024300). Work undertaken at DFM was funded by the Danish Agency for Institutions and Educational Grants. NIST work was funded solely by the United States Government. The authors acknowledge technical advice on the protocol development from Andrew Pollard, Caitlin Thomson, Filipe Richheimer and Alexander G. Shard (NPL).

Disclosure

Certain commercial equipment, instruments, software or materials are identified in this paper in order to specify the experimental procedure adequately. Such identifications are not intended to imply recommendation or endorsement by the National Institute of Standards and Technology (NIST), nor is it intended to imply that the materials or equipment identified are necessarily the best available for the purpose.

Conflicts of Interest

The authors declare no conflicts of interest.

Data Availability Statement

The data that support the findings of this study are available from the corresponding author upon reasonable request.

References

1. Z. Yang, X. Wang, W. Chen, et al., "Residual Stress Characterization in Microelectronic Manufacturing: An Analysis Based on Raman Spectroscopy," *Laser & Photonics Reviews* 18 (2024): 2301300.

2. S. Wood, J. R. Hollis, and J.-S. Kim, "Raman Spectroscopy as an Advanced Structural Nanoprobe for Conjugated Molecular Semiconductors," *Journal of Physics D: Applied Physics* 50 (2017): 073001.

3. K. S. Lee, Z. Landry, F. C. Pereira, et al., "Raman Microspectroscopy for Microbiology," *Nature Reviews Methods Primers* 1 (2021): 80.

4. Y. Wang, L. Fang, Y. Wang, and Z. Xiong, "Current Trends of Raman Spectroscopy in Clinic Settings: Opportunities and Challenges," *Advancement of Science* 11 (2024): 2300668.

5. S. Guo, C. Beleites, U. Neugebauer, et al., "Comparability of Raman Spectroscopic Configurations: A Large Scale Cross-Laboratory Study," *Analytical Chemistry* 92 (2020): 15745–15756.

6. A. Raj, C. Kato, H. A. Witek, and H. Hamaguchi, "Toward Standardization of Raman Spectroscopy: Accurate Wavenumber and Intensity Calibration Using Rotational Raman Spectra of H2, HD, D2, and Vibration–Rotation Spectrum of O2," *Journal of Raman Specroscopy* 51 (2020): 2066–2082.

7. D. Liu and B. M. Hennelly, "Improved Wavelength Calibration by Modeling the Spectrometer," *Applied Spectroscopy* 76 (2022): 1283–1299.

8. T. Bocklitz, T. Dörfer, R. Heinke, M. Schmitt, and J. Popp, "Spectrometer Calibration Protocol for Raman Spectra Recorded With Different Excitation Wavelengths," *Spectrochimica Acta. Part A, Molecular and Biomolecular Spectroscopy* 149 (2015): 544–549.

9. J. D. Rodriguez, B. J. Westenberger, L. F. Buhse, and J. F. Kauffman, "Standardization of Raman Spectra for Transfer of Spectral Libraries Across Different Instruments," *Analyst* 136 (2011): 4232–4240.

10. A. Ntziouni, J. Thomson, I. Xiarchos, et al., "Review of Existing Standards, Guides, and Practices for Raman Spectroscopy," *Applied Spectroscopy* 76, no. 7 (2022): 747–772.

11. International Organization for Standardization, "ISO 18516:2019 "Surface Chemical Analysis—Determination of Lateral Resolution and Sharpness in Beam Based Methods With a Range From Nanometres to Micrometres"," ISO, Geneva, (2019).

12. N. J. Everall, "Confocal Raman Microscopy: Performance, Pitfalls, and Best Practice," *Applied Spectroscopy* 63 (2009): 245A–262A.

13. N. Everall, I. Priestnall, P. Dallin, et al., "Measurement of Spatial Resolution and Sensitivity in Transmission and Backscattering Raman Spectroscopy of Opaque Samples: Impact on Pharmaceutical Quality Control and Raman Tomography," *Applied Spectroscopy* 64 (2010): 476–484.

14. International Organization for Standardization, "ISO 18337:2015. "Surface Chemical Analysis—Surface Characterization—Measurement of the Lateral Resolution of a Confocal Fluorescence Microscope"," ISO, Geneva, (2015).

15. N. Itoh and N. Hanari, "Reliable Evaluation of the Lateral Resolution of a Confocal Raman Microscope by Using the Tungsten-Dot Array Certified Reference Material," *Analytical Sciences* 36 (2020): 1009–1013.

16. T. Peach, "Chapter 7—Self Assembled Single Si Nanowire Transistors," in *Bismuth Implantation and Fabrication Routes Towards Silicon Donor Based Quantum Technologies*, PhD Thesis, (University of Surrey, 2022).

17. M. Constantinou, G. P. Rigas, F. A. Castro, et al., "Simultaneous Tunable Selection and Self-Assembly of Si Nanowires From Heterogeneous Feedstock," *ACS Nano* 10, no. 4 (2016): 4384–4394.

18. A. Y. René Schödel and A. Lewis, "The New Mise en Pratique for the Metre—A Review of Approaches for the Practical Realization of Traceable Length Metrology From 10−11 m to 1013 m," *Metrologia* 58 (2021): 052002.

19. R. L. Farrow, R. K. Chang, S. Mroczkowski, and F. H. Pollak, "Detection of Excess Crystalline as and Sb in III-V Oxide Interfaces by Raman Scattering," *Applied Physics Letters* 31 (1977): 768–770.

20. R. Tanta, M. H. Madsen, Z. Liao, et al., "Raman Spectroscopy and Electrical Properties of InAs Nanowires With Local Oxidation Enabled by Substrate Micro-Trenches and Laser Irradiation," *Applied Physics Letters* 107 (2015): 243101.

21. VAMAS, "Versailles Project on Advanced Materials and Standards (VAMAS)," accessed 2024, http://www.vamas.org/.

22. The MathWorks Inc, "MATLAB. Version 24.2.0 (R2024b)," Natick, Massachusetts, (2024).

23. R. Tanta, T. Kanne, F. Amaduzzi, et al., "Morphology and Composition of Oxidized InAs Nanowires Studied by Combined Raman Spectroscopy and Transmission Electron Microscopy," *Nano* 27 (2016): 305704.

24. M. B. Johnston and H. J. Joyce, "Polarization Anisotropy in Nanowires: Fundamental Concepts and Progress Towards Terahertz-Band Polarization Devices," *Progress in Quantum Electronics* 85 (2022): 100417.

25. F. Lagugné-Labarthet, "Polarized Measurements in Raman Microsopy," *Annual Reports Section "C" (Physical Chemistry)* 103 (2007): 326–350.

26. International Organization for Standardization, *ISO 23124:2024 Surface Chemical Analysis—Measurement of Lateral and Axial Resolutions of a Raman Microscope* (ISO, 2024).

Supporting Information

Additional supporting information can be found online in the Supporting Information section. **Data S1:** Supporting information.